Int. J. Heat Mass Transfer. Vol. 5, pp. 903–914. Pergamon Press 1962. Printed in Great Britain.

STABILITY AND TRANSITION OF THE FREE-CONVECTION LAYER ALONG A VERTICAL FLAT PLATE

ALBIN A. SZEWCZYK*
Institute for Fluid Dynamics and Applied Mathematics
University of Maryland, College Park, Maryland

(*Received* 7 *August* 1961 *and in revised form* 12 *March* 1962)

Abstract—The free-convection layer along a vertical flat plate is investigated theoretically as well as experimentally with a view to studying its instability and "natural" transition from laminar to turbulent flow. Stability calculations are carried out based upon the small perturbation theory for the exact velocity profile for the Prandtl number 10. Temperature profiles are measured along a vertical electrically heated brass plate in good agreement with the theory. By use of the dye technique the natural transition mechanism is investigated, i.e. onset of wave-motion, and subsequent distortion into three-dimensional pattern and also eventual breakdown are studied. A double-row vortex system arises in the free-convection layer. The wave-motion initially provoked outside the velocity maximum is found to be far more unstable than that formed inside the velocity maximum. Its mechanics and overall effect on the stability and transition of the free-convection layer are discussed. The transition process is quite similar to that already observed in the ordinary boundary layer.

NOMENCLATURE

B_n, arbitrary constant;
c, wave propagation speed;
c_p, specific heat at constant pressure;
Fr, Froude number;
f, dimensionless stream function;
f', dimensionless velocity;
g, gravitational constant;
G, modified Grashof-number parameter based on x;
Gr_x, Grashof number based on x;
k, coefficient of heat conductivity;
p, total pressure;
P, pressure of the basic flow;
Pr, Prandtl number;
Ra, Rayleigh number;
t', temperature perturbation function;
t, absolute temperature;
t_∞, ambient temperature;
t_w, wall temperature;
z, dimensionless independent variable;
u, velocity parallel to surface;
U, velocity of basic flow;
v, velocity normal to surface;
x, distance from leading edge of the plate;
y, normal distance from surface;
$\tilde{}$, disturbance quantity;
$(^-)$, dimensional quantity.

Greek symbols

α, wave-number;
β, coefficient of volumetric expansion;
δ, boundary-layer thickness;
ϵ, small parameter;
η, dimensionless similarity variable;
θ, dimensionless disturbance temperature function;
ϑ, dimensionless temperature function;
λ, wavelength of disturbance wave;
μ, viscosity;
ν, kinematic viscosity;
ξ, dimensionless temperature amplitude function;
ρ, density;
τ, time;
ϕ, dimensionless velocity amplitude function;
ψ, stream function.

Subscripts

c, neighborhood of critical layer;
i, refers to inner critical layer;
o, refers to outer critical layer;
0, w, evaluated at the wall.

* Research Associate.

INTRODUCTION

TRANSITION from laminar to turbulent flow has drawn the attention of many investigations throughout the years. In most of the experimental as well as theoretical studies, over-all effects of certain imposing conditions on transition have been investigated. Many details of the actual mechanism of transition, however, still remain unknown. In recent years investigations have been centered on clarifying the intricate mechanism of transition through experimental studies.

Experimental studies have been greatly enhanced by the development of the small-disturbance stability theory. Although the stability theory provides no insight into the actual mechanism of transition, it does determine under what conditions certain small disturbances would amplify or decay in a given flow.

The present investigation was initiated in order to attain a better basic understanding of the "natural transition" process in contrast to the artificially stimulated transition process as studied by Schubauer and Skramstad [1], Schubauer and Klebanoff [2], Klebanoff and Tidstrom [3], Hama *et al.* [4] and Hama [5]. The free-convection layer along a vertical flat plate affords an excellent opportunity of studying the phenomena associated with "natural transition".

Eckert and Soehnghen [6] and Eckert *et al.* [7] investigated the transition process in the free-convection layer along a heated vertical flat plate in air using an interferometer. The interferograms, however, restricted the observations to only a two-dimensional picture. Since the transition process is intrinsically three-dimensional, only a limited understanding of the transition process was obtained.

Birch [8] and Gartrell [9] introduced controlled disturbances into the flow about an isothermal wall. They attempted to find a relation among the various flow parameters which could be used to predict the effect of variations in flow conditions and disturbances on free-convection flows. However, they found empirical relations which hold only to their specific test conditions and not to free-convection flows generally.

Recently, Eckert *et al.* [10] studied the three-dimensional process of natural transition in a free-convection layer by the introduction of smoke threads into the heated layer. Vortex formation and break-up were studied visually and recorded in motion pictures. Some quantitative evaluations and effects of a single roughness element on the free-convection flow were also presented.

Other experiments on transition in the free-convection fields over vertical flat plates and cylinders were performed by Saunders [11, 12], Hermann [13], Fujii [14] and Larson [15]. These authors, however, were essentially concerned with the transition Rayleigh number. They found that transition took place at the Rayleigh number approximately $2\text{–}4 \times 10^9$ in various fluids.

Lack of theoretical investigations into the instability of free-convection flow provided an additional reason for careful analysis of the problem. Plapp [16] performed an analysis on a polynomial approximation of the free-convection velocity profile in air. In addition to obtaining a neutral stability curve for the polynomial profile, he also obtained a portion of the neutral stability curve for the exact velocity profile. However, it was desired in the present investigation to obtain a more accurate solution based upon the exact velocity for a larger Prandtl number corresponding to water.

THEORETICAL ANALYSIS

Consider a steady-state free-convection flow about a vertical heated plate. Physical flow configuration and co-ordinate system are shown in the sketch on the facing page.

The horizontal and vertical components of velocity are designated by u and v, the hydrodynamic pressure by p and the temperature by t.

Stability of the basic free-convection flow will be examined by the method of small perturbations inquiring whether a certain disturbance, which is superposed to the basic flow and which satisfies the equation of motion, is amplified or damped out. A fundamental assumption conventionally adopted in the stability theory is the "parallel flow" condition which stipulates that the mean velocity U depends upon y only in the region where the stability criterion is examined.

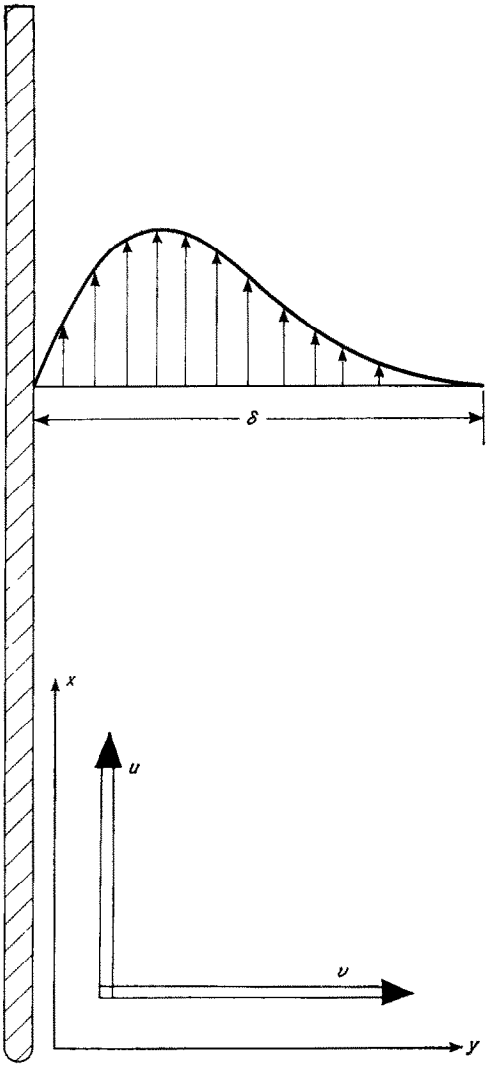

The free-convection flow is a boundary-layer flow which can be well approximated by the parallel-flow concept, because the variation of u with respect to x is much smaller than with respect to y. The basic flow is now described by $U = U(y)$, $V = 0$, $P(y)$ and $T(y)$ and is assumed to be a solution of the steady-state equations.

Superimposed upon the basic flow is a two-dimensional disturbance varying in time and space. When the disturbance velocity components, pressure and temperature are denoted by $\tilde{u}(x, y, \tau)$, $\tilde{v}(x, y, \tau)$, $\tilde{p}(x, y, \tau)$, $\tilde{t}(x, y, \tau)$, the resulting motion is given by $u = U + \tilde{u}$; $v = \tilde{v}$; $p = P + \tilde{p}$; $t = T + \tilde{t}$. The governing equations are:

$$\frac{\partial u}{\partial x} + \frac{\partial v}{\partial y} = 0, \tag{1}$$

$$\frac{\partial u}{\partial \tau} + u\frac{\partial u}{\partial x} + v\frac{\partial u}{\partial y} = -\frac{\partial p}{\partial x} + \nu\nabla^2 u + g\beta(t - t_\infty), \tag{2}$$

$$\frac{\partial v}{\partial \tau} + u\frac{\partial v}{\partial x} + v\frac{\partial v}{\partial y} = -\frac{\partial p}{\partial y} + \nu\nabla^2 v, \tag{3}$$

$$\frac{\partial t}{\partial \tau} + u\frac{\partial t}{\partial x} + v\frac{\partial t}{\partial y} = \frac{k}{\rho c_p}\nabla^2 t, \tag{4}$$

where

$$\nabla^2 = \frac{\partial^2}{\partial x^2} + \frac{\partial^2}{\partial y^2}.$$

The continuity equation is satisfied by introducing a perturbation stream function

$$\tilde{\psi}(x, y, \tau) = \bar{\phi}(y)\, e^{i\bar{a}(x - \bar{c}\tau)} \tag{5}$$

such that

$$\tilde{u} = \frac{\partial \tilde{\psi}}{\partial y} = \bar{\phi}'(y)\, e^{i\bar{a}(x - \bar{c}\tau)}, \tag{6}\dagger$$

$$\tilde{v} = -\frac{\partial \tilde{\psi}}{\partial x} = -i\bar{a}\bar{\phi}(y)\, e^{i\bar{a}(x - \bar{c}\tau)}, \tag{7}$$

where $\bar{\phi}$ is a complex amplitude function of the disturbance, $\bar{a} = 2\pi/\lambda$ is a real positive quantity and represents the wavenumber of the disturbance, whereas $\bar{c}$ is complex, $\bar{c} = \bar{c}_r + i\bar{c}_i$ in which $\bar{c}_r$ denotes the propagation velocity of the disturbance wave in the x-direction and $\bar{c}_i$ denotes the amplification factor. Depending upon whether $\bar{c}_i$ is positive, zero or negative, the wave is amplified, neutral or damped out. In a similar manner a temperature perturbation may be expressed as

$$\tilde{t}(x, y, \tau) = \bar{\xi}(y)\, e^{i\bar{a}(x - \bar{c}\tau)}. \tag{8}$$

It is also appropriate to introduce the following dimensionless variables by dividing all of the quantities involved by characteristic quantities:

$$\eta = y/\delta,$$

† Primes denote differentiation with respect to the independent variable.

where

$$\delta = x\sqrt{(2)}/(Gr_x)^{1/4} \quad \text{and} \quad Gr_x = g\beta\Delta t x^3/\nu_\infty^2, \tag{9}$$

$$f' = Ux/2\nu_\infty\sqrt{Gr_x}, \tag{10}$$

$$\vartheta = (t - t_\infty)/(t_w - t_\infty), \tag{11}$$

$$\phi = \bar{\phi}x/2\nu_\infty\delta\sqrt{Gr_x}, \tag{12}$$

$$\xi = \bar{\xi}/(t_w - t_\infty), \tag{13}$$

$$c = \bar{c}x/2\nu_\infty\sqrt{Gr_x}, \tag{14}$$

$$a = \bar{a}\delta. \tag{15}$$

Substituting equations (5–15) into equations (1–4) and neglecting the nonlinear terms with respect to ϕ and ξ, we obtain

$$(f' - c)(\phi'' - a^2\phi) - f'''\phi = -\frac{i}{aG}(\phi'''' - 2a^2\phi'' + a^4\phi) - \frac{i\beta\Delta t}{aFr}\xi', \tag{16}$$

$$(f' - c)\xi - \phi\vartheta' = -\frac{i}{aGPr}(\xi'' - a^2\xi) \tag{17}$$

where $G = 2\sqrt{(2)}\,(Gr_x)^{1/4}$ is a modified Grashof-number parameter appropriately describing the free-convection flow analogous to the Reynolds number in the conventional boundary layer, $Fr = 4\nu_\infty^2 Gr_x/g\delta x^2$ the Froude number and $Pr = \mu c_p/k$ the Prandtl number. Equations (16) and (17) were derived previously by Plapp [16] by means of a different non-dimensionalizing scheme. Equation (16) is the equivalent of the Orr–Sommerfeld equation† with an additional contribution due to the body-force term, provided the Reynolds number in the conventional Orr–Sommerfeld equation is defined as $Re = U^*\delta/\nu_\infty$ where $U^* = 2\nu_\infty\sqrt{(Gr_x)}/x$. Equation (17) is the counterpart of the Orr–Sommerfeld equation for the temperature fluctuation. The boundary conditions for these equations in the case of an isothermal wall are:

$$\left.\begin{aligned} &\phi(0) = \phi'(0) = \xi(0) = 0, \\ &\phi, \phi', \xi \to 0 \quad \text{as} \quad \eta \to \infty. \end{aligned}\right\} \tag{18}$$

The effect of the density fluctuation appears in the additional body-force term $i\beta\Delta t\xi'/aFr$ which couples equations (16) and (17). When the previous definitions are further substituted in the coefficient of the body-force term, it is easily shown that

$$\frac{\beta\Delta t}{aFr} = \frac{1}{aG} \tag{19}$$

is identical with the coefficient of the viscous-force term. Therefore, as far as the fundamental perturbation equation (16) is concerned, the body-force term and the viscous-force term are of the same order of magnitude. As will be shown below, however, the body-force term does not come into the stability computation. Hence, the stability analysis of the free-convection flow is equivalent to dealing with the conventional Orr–Sommerfeld equation without the body-force term.

(i) *The inviscid solution*

The inviscid solutions are expected to be valid for large values of the Grashof number. As $aG \to \infty$, equation (16) by the virtue of equation (19) reduces to

$$(f' - c)(\phi'' - a^2\phi) - f'''\phi = 0. \tag{20}$$

As a result of the inviscid approximation, singularities arise in equation (20) at the critical points where $f' = c$. The velocity profile in the free-convection flow as shown in the previous sketch has two critical points in contrast to only one critical point in the usual boundary layers. This fact gives additional complications in stability analysis of the free-convection layer. The inner critical point η_{ci} located nearest the wall, whereas the outer critical point η_{co} is located outside the velocity maximum near the ambient fluid. The slope of the velocity profile, f'', is positive at η_{ci} and is negative at η_{co}.

The solutions in the neighborhood of η_c as given by Gregory *et al* [18], who considered a family of velocity profiles of which the free-convection profile is a typical one, are in the form

$$\phi_1 = (\eta - \eta_c)\sum_{n=0}^{\infty} a_n(\eta - \eta_c)^n, \tag{21}$$

$$\phi_2 = \sum_{n=0}^{\infty} b_n(\eta - \eta_c)^n + \frac{f_c'''}{f_c''}\phi_1 \log(\eta - \eta_c). \tag{22}$$

The way of choosing the proper branch of the

† For details see Lin [17].

logarithmic term has been established by earlier workers. (See Lin [17], p. 130.)

(ii) *Viscous solutions*

Seeking a good representation of the solutions in the vicinity of the critical points, where $f' - c$ can be replaced by $f_c''\eta$ and f''' by f_c''', a new variable $z = (\eta - \eta_c)/\epsilon$ is introduced. The parameter ϵ provides a stretching of the coordinate system and is generally considered small for neutral oscillations. ϵ is to be chosen so that at least the largest terms are kept on both sides of equation (16). Thus only the terms $(1/\epsilon^4)\phi''''$ on the right-hand side and $i\alpha G(f' - c)(1/\epsilon^2)\phi''$ on the left-hand side are retained. This is the reason why the body-force term again drops out.

The parameter ϵ becomes $\epsilon_i = (\alpha G f_{ci}'')^{-1/3}$ in the neighborhood of η_{ci} and $\epsilon_0 = (\alpha G/f_\infty'')^{-1/3}$ in the neighborhood of η_{co}. The viscous solutions are given as (see Lin [17] for details)

$$\phi_3 = \int_\infty^z \int_\infty^z z^{1/2} H_{1/3}^{(1)} [\tfrac{2}{3}(iz)^{3/2}]\, dz\, dz, \quad (23)$$

$$\phi_4 = \int_{-\infty}^z \int_{-\infty}^z z^{1/2} H_{1/3}^{(2)} [\tfrac{2}{3}(iz)^{3/2}]\, dz\, dz, \quad (24)$$

where $H_{1/3}^{(1)}$ and $H_{1/3}^{(2)}$ denote the Hankel functions of the first and second kinds of order one-third, respectively.

(iii) *The eigenvalue equation*

The eigenvalue equation is obtained by substituting a linear superposition of $\phi_{1,2,3,4}$ in the boundary-condition equation (18). Since the Hankel Function $H_{1/3}^{(2)}$ goes to infinity as $z \to \infty$, it does not satisfy the boundary condition at infinity. Therefore ϕ_4 should not contribute to the solution, and we have the following set of algebraic equations for constants B_1, B_2 and B_3;

$$\left.\begin{aligned} &B_1\phi_1(0) + B_2\phi_2(0) + B_3\phi_3(0) = 0,\\ &B_1\phi_1'(0) + B_2\phi_2'(0) + B_3\phi_3'(0) = 0,\\ &B_1\phi_1(\infty) + B_2\phi_2(\infty) + B_3\phi_3(\infty) = 0. \end{aligned}\right\} \quad (25)$$

The Hankel function $H_{1/3}^{(1)}$ vanishes as $z \to \infty$, and consequently $\phi_3(\infty) \to 0$. Choosing ϕ_1 so that $\phi_1(\infty) = 0$, we have $B_2 = 0$, and thus the system of equations reduces to

$$\left.\begin{aligned} &B_1\phi_1(0) + B_3\phi_3(0) = 0,\\ &B_1\phi_1'(0) + B_3\phi_3'(0) = 0. \end{aligned}\right\} \quad (26)$$

Substituting the independent variables z_{i_0} and z_{o_0} leads to the eigenvalue equation

$$-\frac{\phi_1(0)}{\eta_{ci}\phi_1'(0)} = \frac{\phi_3(z_{i_0})}{z_{i_0}\phi_3'(z_{i_0})}, \quad (27)$$

when the inner-critical point is considered, and

$$-\frac{\phi_1(0)}{\eta_{co}\phi_1'(0)} = \frac{\phi_3(z_{o_0})}{z_{o_0}\phi_3'(z_{o_0})} \quad (28)$$

for the outer-critical point. Appendix A describes the computational procedure for the inviscid function $\phi_1(0)/\phi_1'(0)$. The eigenvalue equation (27) is conventional. Equation (28) concerning the outer-critical point, however, gives only a rough approximation of the desired solution. In the stability analysis the first term of the Taylor series expansion for $(f' - c)$ is retained, i.e. the local slope of the velocity profile at the critical point is projected to the wall. This procedure results in a large deviation from the actual velocity at the wall when applied to the outer-critical layer, whereas for the inner critical layer reasonable agreement is obtained at the wall. Therefore, even if the same mathematical procedure is applied to the stability criterion based upon the inner and outer critical points, the results due to the latter are inherently a rougher approximation.

EXPERIMENTAL EQUIPMENT

The experiments were performed in a water tank 3 ft wide, 5 ft deep and 7 ft long. A vertical heated plate was made of brass 31 in wide, 60 in long and 0·25 in thick. The brass plate was one side of a double-wall construction which was mounted in a bakelite frame. The entire brass plate was heated by two circuits of No. 22 Nichrome wire. A variac controlled the current of the 0–15 A circuits within 0·1 A.

In order to facilitate the analysis of experimental results, a grid consisting of 5 × 5 cm squares was marked on the brass plate starting at 30 cm from the leading edge. The temperature of the plate was determined from thirteen thermocouples imbedded in the plate. All thermocouples used in this experiment had

copper–constantan junctions. The temperature field in the free-convection layer created by the heated wall was measured by a thermocouple probe as shown in Fig. 1. The thermocouple probe was attached to a traversing mechanism, as shown in Fig. 2. The traversing mechanism had an accuracy of traverse of 0·0005 in.

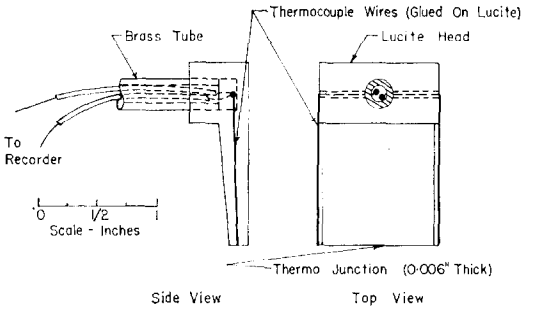

FIG. 1. Thermocouple probe.

The thermocouple readings were recorded by a Leeds and Northrup Speedomax recorder. Actual temperatures were printed on temperature-co-ordinate paper having a scale of 0–50°C. They could be read within the accuracy of approximately 0·05 degC.

For the study of the stability and transition of the free-convection layer, the flow visualization technique of dye injection was used. Analine dyes were injected smoothly through three different types of dye rakes. For plan-view observation of the flow development, hypodermic dye rakes as shown in Fig. 3 allowed black dye or black and red dye to be injected into the free-convection layer. A comb-type dye rake or an individual hypodermic needle was used for side-view observations. The comb-type rake emitted several colors of dye at various distances from the wall in a single plane so as to identify different flow paths at various distances from the wall. The flow experienced no ill effects from the dye rakes inserted into the flow field 6 in from the leading edge.

Flow phenomena were analysed from both motion pictures and still photographs.

RESULTS, OBSERVATIONS AND DISCUSSION

Typical results of the temperature-profile measurements are plotted non-dimensionally in Fig. 4. The wall temperature was obtained by averaging the temperatures recorded from the imbedded thermocouples. This average wall temperature was in close agreement in nearly all instances with the temperature obtained by extrapolating the temperature profile to the wall. The local wall temperature also was in close agreement with the over-all average wall temperature. A typical wall temperature distribution is given in Fig. 5. Near the leading edge of the wall there is a flow-wise temperature gradient in the wall owing to a more intense cooling effect in this region. The wall temperature, nevertheless, approaches an almost uniform value rapidly and the effect due to the small gradient near the leading edge is neglected; the two temperature readings obtained in the first 5 in are not included in averaging the wall temperature.

The fluid properties included in the definition of the dimensionless variable η are evaluated at the ambient temperature t_∞. Since the temperature difference between the wall and ambient temperature was small, the values of η did not

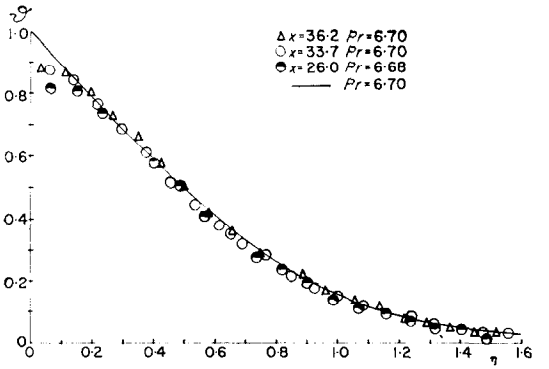

FIG. 4. Dimensionless temperature profiles.

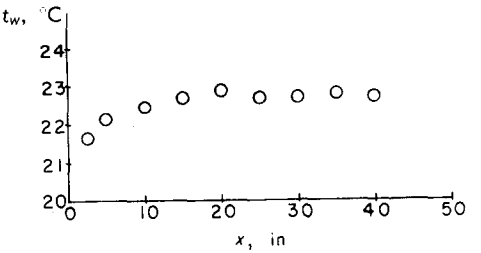

FIG. 5. Typical wall temperature distribution.

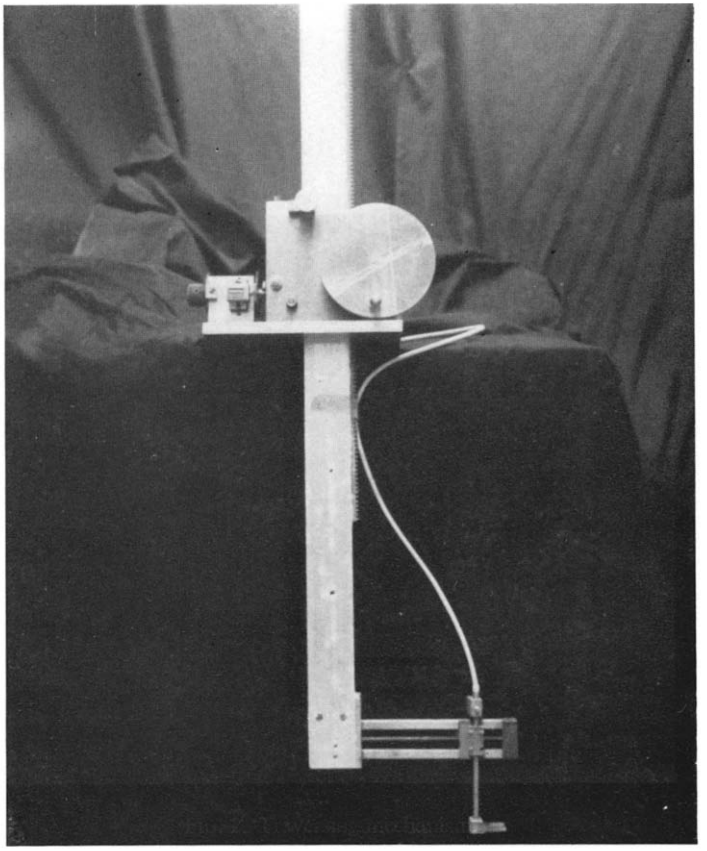

FIG. 2. Traversing mechanism.

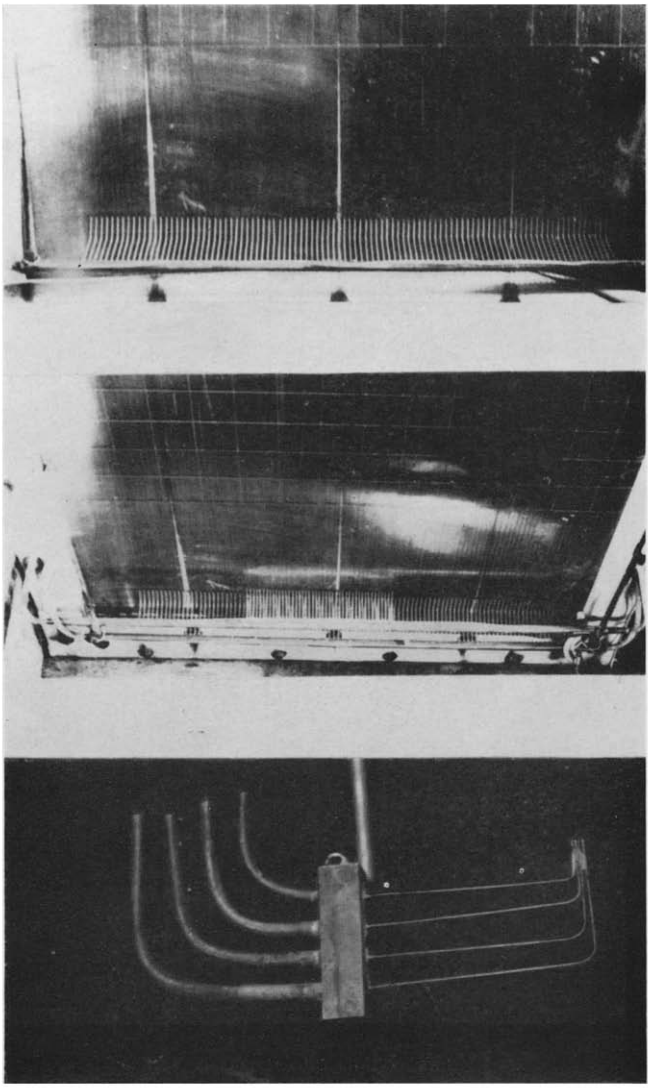

FIG. 3. Dye rakes and dye comb.

change appreciably even when the fluid properties were evaluated with the wall temperature as a reference temperature. Therefore, this is an arbitrary yet non-essential choice as long as the temperature difference remains small.

The experimental results are compared with the theoretical temperature profiles interpolated from those calculated by Ostrach [19] for various Prandtl numbers. Agreement between the theoretical and experimental temperature profiles is excellent.

Equations (27) and (28) were solved for the velocity profile corresponding to a Prandtl number of 10, since it was assumed that it would provide an upper bound for a good representative velocity profile for the free-convection flow in water. The solutions of equations (27) and (28), which refer to the inner and outer critical points, are plotted in Fig. 6 and Fig. 7, respectively. The indifference curves obtained from the intersection points on Fig. 6 and Fig. 7 are plotted in Fig. 8. Based on the inner-critical point the minimum value of G was obtained to be $3{\cdot}46 \times 10^5$ corresponding to $c = 0{\cdot}0235$ and $\alpha = 0{\cdot}875$. On the other hand, in spite of the approximation procedure in regard to the velocity profile for the outer-critical point in the stability calculations, somewhat more reasonable values for G were obtained. The lowest value of G obtained was $G = 5040$ at $c = 0{\cdot}005$ and $\alpha = 1{\cdot}5$. A marked shift in this portion of the neutral stability curve is noted and a more reasonable critical value is implied in these results.

Experimental results for the minimum observable wavelengths and the wave speeds are plotted in Figs. 8 and 9. Although the agreement between the measured minimum modified Grashof-number parameter and that predicted by theory based on the inner critical layer is poor, there is a fairly good agreement between the measured α and c, and those corresponding to the minimum value of G. Comparing the experimental results with the c, α and G values obtained from equation (28), a better agreement in the G parameter is obtained, 8–10 times less than that predicted by the theory. But the α and the c corresponding to this G value provide less satisfactory agreement with experiment.

Within the distance approximately 40 cm from the leading edge, thin black dye streaks move up the surface of the wall very slowly without showing any indication of breaking up. In this distance from the leading edge the flow was laminar. This laminar flow pattern can be seen in the lower portion of Fig. 10 in which the flow direction is from the bottom to top.

At 55 cm from the leading edge a faint two-dimensional dye accumulation begins to appear. A rather concentrated, more definable dye line

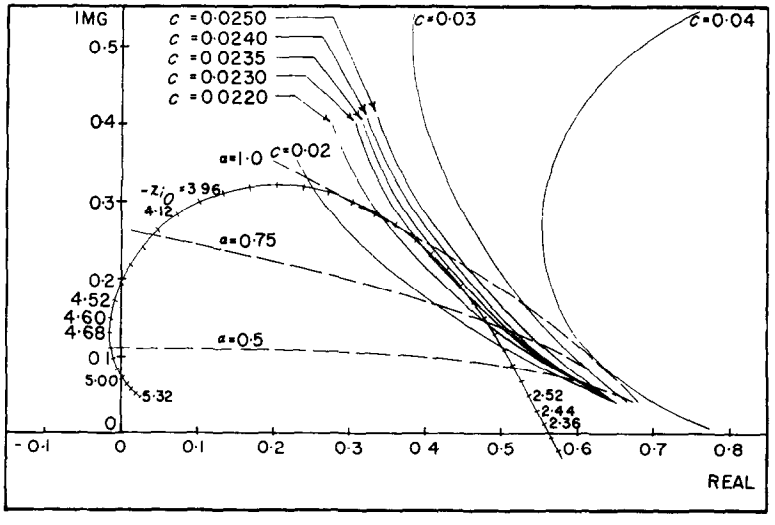

FIG. 6. Solution of equation (27).

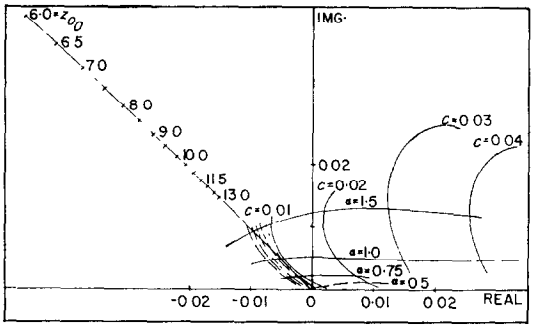

FIG. 7. Solution of equation (28).

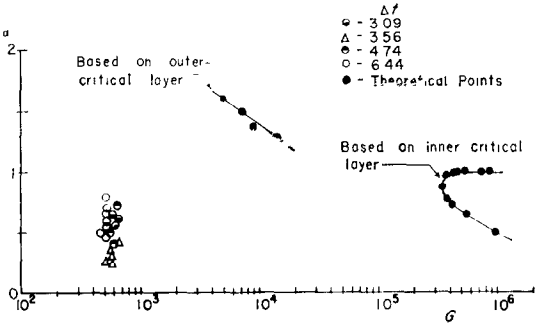

FIG. 8. Indifference curves and experimental data for the wavelengths.

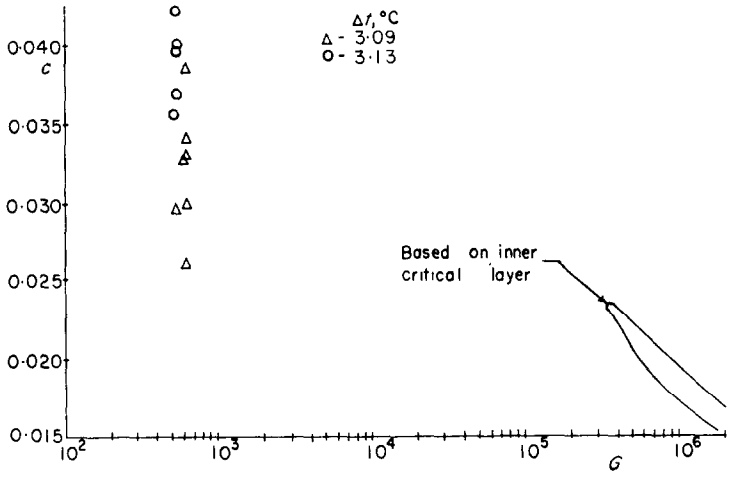

FIG. 9. Indifference curve and experimental data for the wave speed.

is seen at 60 cm, thus giving a wavelength of approximately 5 cm.

The wavelength was obtained by averaging several measurements across the plate, since there was a certain amount of irregular transverse waviness exhibited by the wavefront. This transverse waviness, however, was not unexpected since the disturbance waves occurred naturally and were not produced by an artificial means of any geometrical regularity or at a specific frequency. Since the disturbance waves were formed arbitrarily in time as well as in space, a certain portion of a wave moving downstream could be engulfed by a second wave started at a slightly higher x-location.

As we proceed upwards with the flow in Fig. 10, it is noted that a "splitting" of the dye streaks begins to take place at the wavefront located at $x = 60$ cm. The splitting of the dye streaks appears because there is a secondary twisting of the dye streak near the plate surface. Although this twisting of the dye streak occurs, the free-convection layer still appears to be in a somewhat later stage of a still laminar flow, or in the initial stages of transition.

The dye streaks roll up to form a vortex. This type of vortex rolling-up was demonstrated by Hama [5] for the boundary-layer flow over a flat plate. In all instances observed, the vortex continues to roll up and appears in the plan view as a highly concentrated dye spot for a single dye streak or as a concentrated dye line for several streaks. Such a concentrated dye line is observed in Fig. 10 at $x = 60$ cm. This

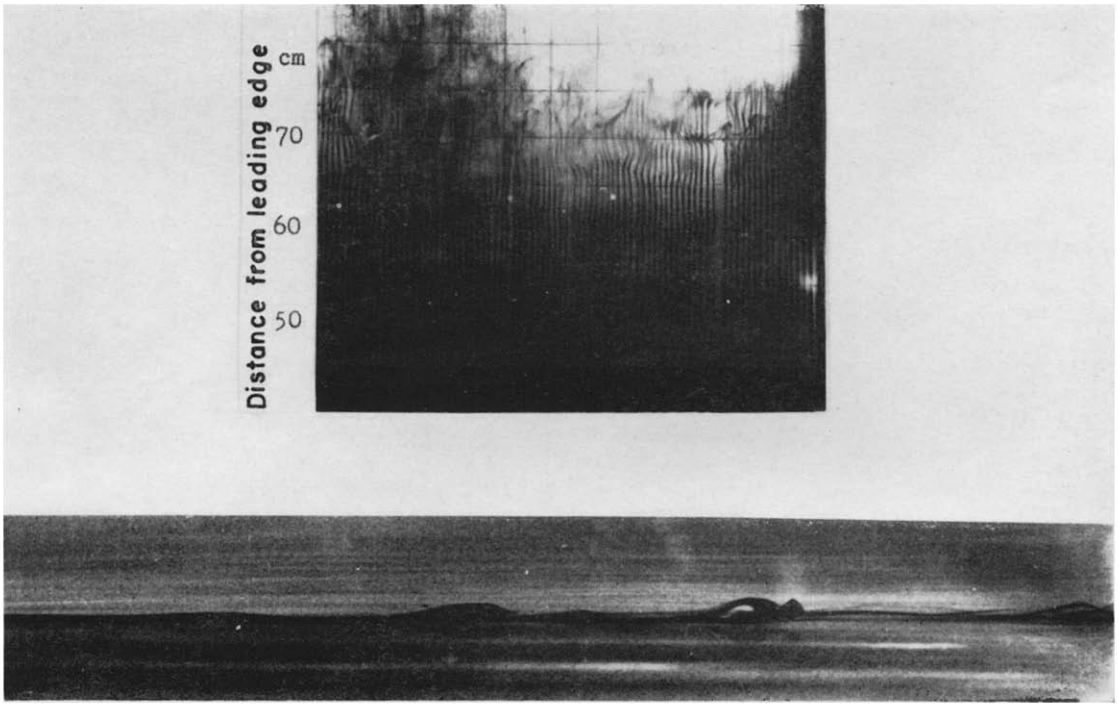

FIG. 10. Plan view and side view of vortex development at $t = 6{\cdot}44°C$, $G = 478$, and $\alpha = 0{\cdot}493$.

f. p. 910

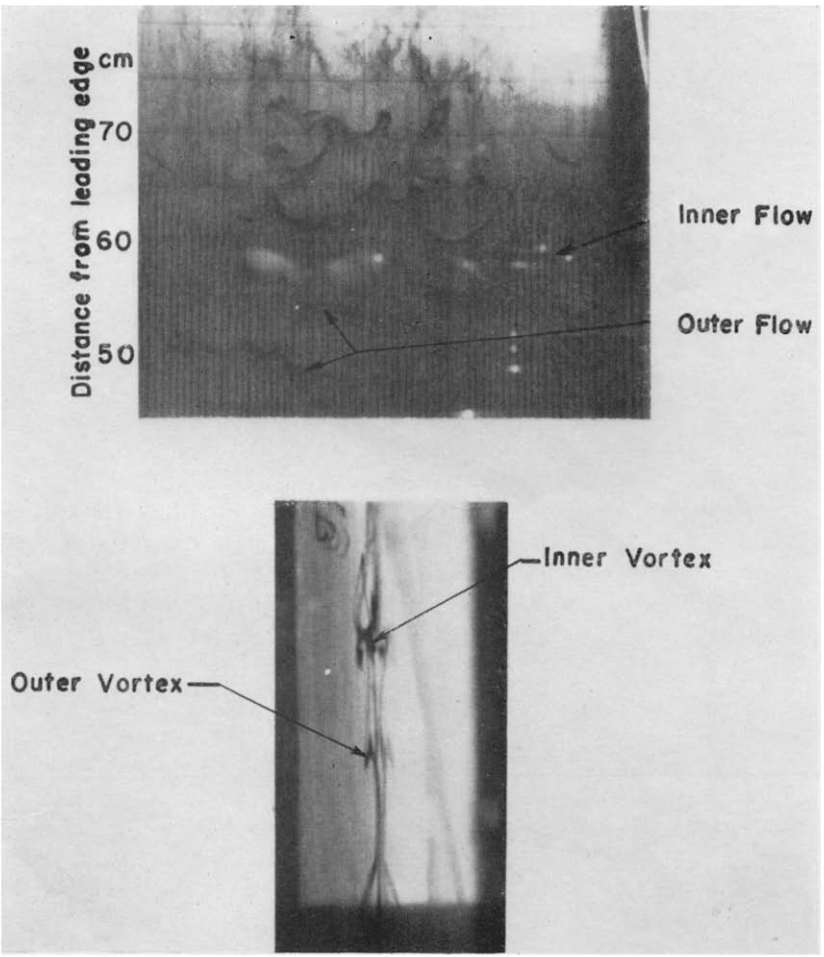

FIG. 11. Double-row vortex system in plan and side view.

concentrated dye line continues to be concentrated and the wave amplified until a second splitting process occurs. The vortex, which appeared to be mainly two-dimensional, now begins to take on some three-dimensional character. Yet, from a side view it appears as a nearly two-dimensional rolling-up, but the plan view clearly shows the distortion into a three-dimensional formation. Before this three-dimensionality proceeds very far down-stream, several dye streaks all having the same character join in forming a vortex loop. The edges of the dye streaks, which form the legs of the loop, are very cloudy and immediately burst into highly random motion indicating the burst of a turbulence spot. Any further observation is completely obscured by the dye clouds due to the random motion.

Observations of single dye streaks from the dye comb produced rather unexpected results. A double-row vortex system is observed. A dye streak rolls up on the wall similar to that observed in conventional boundary-layer flow over a flat plate, whereas a dye streak outside the maximum velocity rolls outward in the opposite direction to that of the vortex formed on the plate. This vorticity distribution in the free-convection layer confirmed the speculation brought forth by Fujii [14], although the actual phase relation between the two vortex rows differs from his sketch. Perhaps, more interesting to note is that Fales [20] observed a similar phenomenon when a jet of clear water issued into a bath of dyed water. A strong similarity exists between a jet velocity profile and the velocity profile obtained for a free-convection layer.

The rolling up of the outer vortex begins to occur near the leading edge. When the outer wavefront appears, the inner dye streaks in the rear riding up the surface of the plate remain laminar as seen in Fig. 11. Several wavefronts of the outer dye streaks are observed in contrast to generally only two or at most three wavefronts observed of the dye streaks on the surface of the plate as previously discussed. As the wave progresses upwards along the plate and appears to be amplified, the outer dye lines become more concentrated. The concentrated outer dye lines exhibit the same type of vortex rolling up as before until again the vortex loop is developed and eventual breakdown occurs. This breakdown observed in the outer layer occurs at a distance from the leading edge when the inner layer is still laminar or only shows signs of initially entering transition. The outside rolling vortex is very strong and impresses its effect onto the inner layer. The inner layer is actually disturbed by the large amplification of the outside disturbance wave and by its development to final breakdown. Hence, the inside wave is provoked by the highly unstable motion occurring outside the maximum velocity. This occurrence must result from the strong instability due to the inflection point in the velocity profile located outside the maximum velocity. The effect of inflectional instability is to overtake the flow completely and to control its behavior. This type of instability was clearly manifested in the breakdown of the free-convection layer from laminar to turbulent flow.

The outside wave so dominated the flow that it impressed its wavelength onto the wave disturbance in the inner layer. The outside wave is completely established even before the inside wave begins to show signs of a vortex rolling up. Experimental data for the outer wave disturbance fall into the same region on the α–G plot as did the previously measured data from the wave very near the wall.

SUMMARY AND CONCLUSIONS

Theoretical as well as experimental investigations of the instability and transition in the free-convection layer along a vertical flat plate have led to the following conclusions:

(1) In the process of natural transition in the free-convection layer a double-row vortex system arises.

(2) The instability due to the outer critical layer is predominant and sets in first, well in advance of the onset of any possible instability due to the inner critical layer.

(3) The outside vortices completely control the behavior of the flow developments and impress their effect onto the more stable inner layer near the surface, provoking its instability.

(4) The above observation explains why the critical Grashof-number parameter experimentally obtained here and in the other literature

is so much below the theoretical Grashof-number parameter $3{\cdot}46 \times 10^5$ which is computed based upon the instability of the inner critical layer. Such an instability simply does not come into the picture.

(5) The theoretical calculations for the minimum Grashof-number parameter based on the inner-critical layer for a velocity profile corresponding to a Prandtl number 10 produces values of Grashof number of the same order of magnitude as obtained by Plapp [16] for a velocity profile corresponding to a Prandtl number of 0·72.

(6) The instability calculation based upon the consideration of the outer critical layer shows a drastic reduction of the theoretical Grashof-number parameter to the order of 10^3.

(7) The transition process in the free-convection flow is essentially the same as observed in other cases. It is somewhat different, however, from that in the ordinary boundary layer over a flat plate as observed recently by Klebanoff. It is believed that, in the free-convection layer as in some other cases, the amplification rate is so high that the discrete vortices appear first before any other nonlinear mechanism begins to show up.

ACKNOWLEDGEMENTS

The author would like to express his sincere appreciation to Dr. Francis R. Hama for his guidance and helpful advice furnished during the course of this investigation, and to Dr. Shan-Fu Shen sincere thanks for his valuable advice and discussion afforded the author in regard to the theoretical aspects of the stability problem. In addition the author gratefully acknowledges the support of the United States Air Force Office of Scientific Research under Contract AF(638)645 which made this research possible.

REFERENCES

1. G. B. Schubauer and H. K. Skramstad, Laminar boundary-layer oscillations and transition on a flat-plate. *J. Res. Nat. Bur. Stand.* **38**, 251 (1947).
2. G. B. Schubauer and P. S. Klebanoff, Contributions on the mechanics of boundary-layer transition, *NACA* Rep. 1289 (1956), (supersedes *NACA* TN-3489, 1955).
3. P. S. Klebanoff and K. D. Tidstrom, Evolution of amplified waves leading to transition in a boundary-layer with zero pressure gradient, *NASA* TN-D-195 (1959).
4. F. R. Hama, J. D. Long and J. C. Hegarty, On transition from laminar to turbulent flow, Inst. Fluid Dyn. Appl. Math., Univ. of Maryland, TN BN-81 (1956); *J. Appl. Phys.* **28**, 388 (1957).
5. F. R. Hama, Boundary-layer transition induced by a vibrating ribbon on a flat plate, Inst. Fluid Dyn. Appl. Math., Univ. of Maryland, TN BN-195 (1960); *Proc.* 1960 *Heat Transfer and Fluid Mechanics Institute*, Stanford Univ., p. 92 (1960).
6. E. R. G. Eckert and E. Soehnghen, Interferometric studies on the stability and transition to turbulence of a free-convection boundary layer. *Proc. General Discussion on Heat Transfer*, London, p. 321 (1951).
7. E. R. G. Eckert, E. Soehngen and P. J. Schneider, Studien zum Umschlag laminar-turbulent der freien Konvektions-Strömung an einer senkrechten Platte, *Fünfzig Jahre Grenzschichtforschung*. Vieweg, Braunschweig (1955).
8. W. D. Birch, On the Stability of Free-Convection Boundary Layers on a Vertical Flat Plate. Thesis, Air University (1957).
9. H. E. Gartrell, On the Oscillations of Free-Convection Boundary Layers. Thesis, Air University (1959).
10. E. R. G. Eckert, J. P. Hartnett and T. F. Irvine, Jr., Flow visualization studies of transition to turbulence in free convection flow, *ASME* Paper No. 60-WA-250 (presented at ASME annual meeting 1960).
11. O. A. Saunders, Effect of pressure upon natural convection in air. *Proc. Roy. Soc.* A **157**, 278 (1936).
12. O. A. Saunders, Natural convection in liquids. *Proc. Roy. Soc.* A **172**, 55 (1939).
13. R. Hermann, Heat transfer by free-convection from horizontal cylinders in diatomic gases, *NACA* TM-1366 (1936).
14. T. Fujii, On the development of a vortex street in a free-convection boundary layer. *Japan Soc. Mech. Engrs*, **2**, 551 (1959).
15. J. R. Larson, Boundary-Layer Transition in Natural Convection. Thesis, University of Washington (1960).
16. J. E. Plapp, Laminar Boundary-Layer Stability in Free Convection—1. Thesis, California Institute of Technology (1957); see also *J. Aero. Sci.* **24**, 318 (1957).
17. C. C. Lin, *Theory of Hydrodynamic Stability*. Cambridge University Press, London (1955).
18. N. Gregory, J. T. Stuart and W. S. Walker, On the stability at three-dimensional boundary layers with application to the flow due to a rotating disk. *Phil. Trans. Roy. Soc. Lond.* A**248**, 155 (1955).
19. S. Ostrach, An analysis of laminar free-convection flow and heat transfer about a flat plate parallel to the direction of the generating body-force, *NACA* TN-2635 (1952) (superseded by Rep. 1111, 1953).
20. E. N. Fales, New laboratory technique for investigation of the origin of fluid turbulence. *J. Franklin Inst.* **259**, 491 (1955).

APPENDIX A

Computation of the Inviscid Function $\phi_1(0)/\phi_1'(0)$ *in Equations* (27) *and* (28)

The inviscid solution ϕ_1 which is in fact a linear combination of two series solutions, is obtained for a chosen combination of α and c from the equation

$$(f' - c)(\phi'' - \alpha^2\phi) - f'''\phi = 0 \quad \text{(A1)}$$

with the boundary conditions

$$\phi(0) = 0, \quad \phi(\infty) = 0. \quad \text{(A2)}$$

For large values of η, $\eta > \eta_{co}$, the derivatives of the velocity profile vanish and the equation reduces to

$$\phi'' - \alpha^2\phi = 0. \quad \text{(A3)}$$

The solutions of equation (A3) are $\phi = e^{\pm\alpha\eta}$. Imposing the condition $\phi(\infty) = 0$, we see that only $\phi = e^{-\alpha\eta}$ is acceptable. Thus the exponential solution gives the necessary starting values to integrate numerically from infinity inward to the wall. A difference scheme was used and integration of the equation

$$\phi'' - \left(\alpha^2 + \frac{f'''}{f' - c}\right)\phi = 0 \quad \text{(A4)}$$

was continued until the neighborhood of the singular point ($f' = c$) was reached. In this neighborhood the solutions are given by

$$\phi_{1c} = (\eta - \eta_c)\sum_{n=0}^{\infty} a_n(\eta - \eta_c)^n, \quad \text{(A5)}$$

$$\phi_{2c} = \sum_{n=0}^{\infty} b_n(\eta - \eta_c)^n + \frac{f_c'''}{f_c''}\phi_{1c}\log(\eta - \eta_c). \quad \text{(A6)}$$

These two series solutions are matched to the value ϕ_1 and the slope ϕ_1' obtained from the numerical integration of equation (A4) at a value of η slightly larger than η_{co}.

The solutions (A5) and (A6), valid only in the neighborhood of η_c, continue the numerical integration for ϕ_1 through the singularity and once again allow the difference scheme to take over the integration for $\eta < \eta_{co}$. The integration is continued until the solution reaches the neighborhood of η_{ci}. Here again the two series solutions as given by equations (A5) and (A6) are matched to the value ϕ_1 and slope ϕ_1'. Once the series solutions have taken us through the second singularity the numerical integration is continued to the wall where $\phi_1(0)$ and $\phi_1'(0)$ are obtained. Thus the inviscid part of the eigenvalue problem $\phi_1(0)/\phi_1'(0)$ is calculated for a given combination of α and c.

Résumé—La convection libre le long d'une plaque plane verticale a été étudiée théoriquement et expérimentalement en vue de contrôler l'instabilité et la transition naturelle du régime laminaire au régime turbulent. Les calculs de stabilité ont été effectués à partir de la théorie de la petite perturbation pour le profil de vitesses exact et un nombre de Prandtl égal à 10. Les profils de températures mesurés sur une plaque de laiton verticale chauffée électriquement sont en bon accord avec la théorie. On a étudié le mécanisme de la transition naturelle par la technique des filets colorés, par exemple, établissement du mouvement ondulatoire et déformation consécutive d'allure tridimensionnelle. Un système tourbillonnaire double se produit dans la couche limite de convection libre. Le mouvement ondulatoire provoqué initialement au-delà du point de vitesse maximum est beaucoup plus instable que celui formé au-dessous de la vitesse maximum. Son mécanisme et son effet sur la stabilité et la transition de la couche limite de convection libre sont étudiés. Le processus de la transition est tout à fait semblable à celui que l'on observe dans les couches limites ordinaires.

Zusammenfassung—Für freie Konvektion an einer senkrechten ebenen Platte wurde die wandnahe Schicht theoretisch untersucht insbesondere auf Instabilität und "natürlichen" Übergang von laminarer in turbulente Strömungsform. Die Stabilitätsberechnungen beruhen auf der Theorie der kleinen Strömungen des exakten Geschwindigkeitsprofils für die Prandtl-Zahl 10. Die an einer elektrisch beheizten senkrechten Messingplatte erhaltenen Temperaturprofile stimmen gut mit der Theorie überein. Mit Hilfe der Färbetechnik wurde der Mechanismus des natürlichen Überganges untersucht, d.h. das Einsetzen der Wellenbewegung, die anschliessende Verzerrung in eine dreidimensionale Form und der eventuelle Zusammenbruch. In der Konvektionsschicht entsteht ein doppelreihiges Wirbelsystem. Die zuerst ausserhalb des Geschwindigkeitsmaximums ausgelöste Wellenbewegung erweist

sich viel instabiler als die innerhalb des Geschwindigkeitsmaximums entstandene. Ihre Mechanik und ihr Gesamteinfluss auf die Stabilität und das Umschlagen in der freien Konvektionsschicht werden diskutiert. Der Umschlagvorgang ist sehr ähnlich dem der gewöhnlichen Grenzschicht.

Аннотация—Изучается теоретически и экспериментально слой свободной конвекции вдоль вертикальной плоской пластины, его неустойчивость и «естественный» переход из ламинарного в турбулентный. На основании теории малых возмущений проводятся расчёты устойчивости для точного профиля скорости, соответствующего значению критерия Прандтля, равному 10. Температурные профили, измеренные вдоль вертикальной электрически нагреваемой латунной пластины, находятся в хорошем соответствии с теорией. Используя метод окрашивания, исследуется механизм естественного перехода, т.е. возникновение волнового движения, последующее разрушение в спектр пространственного обтекания и конечный срыв потока. В слое естественной конвекции возникает система двойного ряда вихрей. Найдено, что волновое движение, вызванное вначале вне максимума скорости, является более неустойчивым, чем возникшее в пределах максимума скорости. Рассматривается механика волнового движения и его влияние на переход слоя свободной конвекции. Процесс перехода полностью напоминает собой процесс, наблюдаемый в обычном пограничном слое.